Enhanced Nonlinear Optical Responses of Layered Epsilon-Near-Zero Metamaterials at Visible Frequencies

Sisira Suresh[1], Orad Reshef[1], M. Zahirul Alam[1], Jeremy Upham[1], Mohammad Karimi[2], and Robert W. Boyd[1,3,*]

[1] *Department of Physics, University of Ottawa, Ottawa, ON K1N 6N5, Canada*
[2] *School of Electrical Engineering and Computer Science, University of Ottawa, Ottawa, ON K1N 6N5, Canada*
[3] *Institute of Optics and Department of Physics and Astronomy, University of Rochester, Rochester, NY 14627, USA*

We demonstrate that a periodic stack of alternating, subwavelength Ag and SiO_2 layers can be designed to place its zero-permittivity wavelength anywhere in the visible. We find that such a metamaterial displays strong nonlinear response in its near-zero-permittivity region, with a Kerr coefficient and nonlinear absorption coefficient as large as $n_2 = (1.2 \pm 0.1) \times 10^{-12}$ m^2/W and $\beta = (-1.5 \pm 0.2) \times 10^{-5}$ m/W, respectively. A theoretical model ascribes these results to an enhancement of the nonlinear coefficients by a factor $1/(n_0 \mathrm{Re}[n_0])$, where n_0 is the linear refractive index.

In recent years, much attention has been given to a class of materials with vanishing dielectric permittivity [1–3]. This class of materials, known as epsilon-near-zero (ENZ) materials, has become a topic of interest because of its intriguing optical properties including tunneling of light through arbitrary bends [1], the ability to tailor radiation patterns [4], and its enhanced nonlinear optical response [5–8]. The ENZ condition can be found in naturally occurring materials near their bulk plasma and phonon resonances. Most noble metals exhibit a zero-permittivity behavior in the UV region, near their respective plasma frequencies [9]. Transition metal nitrides such as titanium nitride [10] and zirconium nitride [11] display their ENZ regime in the visible spectral region. In the near-infrared (NIR) region, doped semiconducting oxides such as tin-doped indium oxide [12] and aluminium-doped zinc oxide [13] behave as ENZ materials. The ENZ condition is also found in silicon carbide [14] and fused silica (SiO_2) [15] in the mid-IR range. The zero-permittivity wavelength of a given material is dictated by its intrinsic material properties, and hence cannot be used for applications that require that the ENZ condition occurs at some specified wavelength. To address this concern, ENZ metamaterials have been developed for use in the microwave [16], IR [2, 17] and visible [18, 19] spectral regions. In homogeneous Drude materials, the nonlinear enhancement of n_2 and β has been thoroughly examined as a function of wavelength in the ENZ region [8]. Although some work has been done exploring the nonlinear response of ENZ metamaterials [20–22], this dependence has yet to be fully characterized. Here, we examine the nonlinear optical response of an ENZ metamaterial that is straightforward to fabricate and for which the ENZ condition can be flexibly set to any targeted wavelength region. We also develop a simple analytic model to explain these results. Our work confirms that a metamaterial indeed does exhibit a nonlinear enhancement in its ENZ region, and therefore, ENZ nonlinear enhancement can be placed at any predefined wavelength.

Our metamaterial is composed of alternating subwavelength-thick layers of metal and dielectric materials. A schematic diagram of the metamaterial geometry is shown in Fig. 1(a). These metamaterials are capable of exhibiting a zero-permittivity wavelength anywhere within the entire visible spectrum by adjusting the respective thicknesses of the constituent materials. At optical frequencies, metals possess a negative dielectric permittivity and dielectrics possess a positive dielectric permittivity. The intuition behind this metamaterial design is, therefore, to form a weighted average of the metal and the dielectric to create an 'effective' ENZ

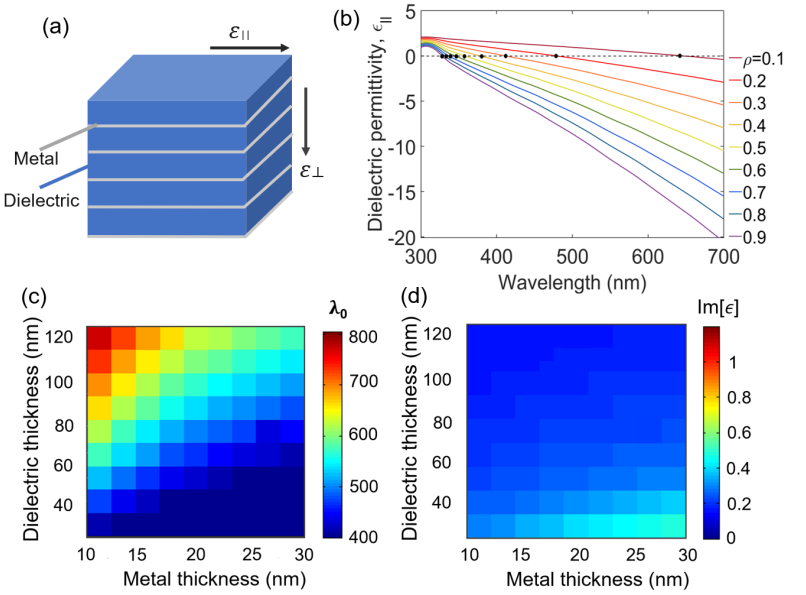

Figure 1: (a) Schematic diagram of a metal-dielectric multilayer stack. (b) Effective parallel permittivities at normal incidence predicted from EMT for different metallic fill fractions (the black circles denote the zero-crossing wavelength for each fill fraction). (c) The zero-permittivity wavelength and (d) the loss of a 5-bilayer Ag-SiO_2 multilayer stack calculated using TMM as a function of the thicknesses of the Ag and SiO_2 layers. Note that the zero-permittivity wavelength can be placed anywhere in the visible region.

medium, provided the inhomogeneity scale of the composite medium is of sub-wavelength dimensions [23–25]. Effective medium theory (EMT) predicts that the wavelength, λ_0, at which the permittivity crosses zero can be evaluated from the fill fraction of the constituents in the composite [26]. Thus, in the limit of sub-wavelength layer thickness, the metal-dielectric multilayer stack can be considered as an effective medium with an effective permittivity for an electric field polarized in the plane of the layers given by $\epsilon_{||} = \rho\epsilon_m + (1-\rho)\epsilon_d$, where ρ is the metallic fill fraction and ϵ_m and ϵ_d are the permittivities of the metal and the dielectric material, respectively [27]. We selected Ag as the metal because of its small damping constant [28], and SiO_2 as the dielectric because of its transparency in the visible spectral region [29]. In Fig. 1(b), the fill fraction is varied from $\rho = 0.1$ to 0.9, and we observe a blue shift in the zero-permittivity wavelength as the metallic fill fraction increases. Thus, the dependence of the zero-permittivity wavelength on the metallic fill fraction should enable an ENZ metamaterial design that can be situated anywhere in the entire visible spectrum.

Although effective medium theory can reliably predict the ENZ wavelength under many situations, this method is rigorously valid only under limiting conditions, such as vanishingly small layer thickness and an infinitely thick overall medium [30]. In order to validate our EMT approach, we perform parameter retrieval using the transfer matrix method (TMM) to aid in our design [31]. Using this method, one can solve for the effective refractive index and consequently the complex effective permittivity of a medium. The TMM simulations reveal optimal designs in terms of zero-permittivity wavelength and optical losses (Fig. 1(c)). We select a design for the Ag-SiO_2 multilayer stack that has both a desired zero-permittivity wavelength and a small amount of loss, consisting of 5 bilayers of Ag and SiO_2 with thicknesses of 16 nm and 65 nm, respectively, for a total thickness of 405 nm. Figure 2(a) depicts the dielectric permittivity at normal incidence as a function of wavelength calculated using both the TMM and EMT methods. The optical losses are due to the resistive losses of silver. This geometry corresponds to a metamaterial with an effective zero-permittivity wavelength of 509 nm, with an imaginary part of dielectric permittivity Im[ϵ] of 0.2.

Having established a preferred design, we fabricated a device for characterization. The Ag and SiO_2 layers were deposited using electron-beam evaporation on a glass

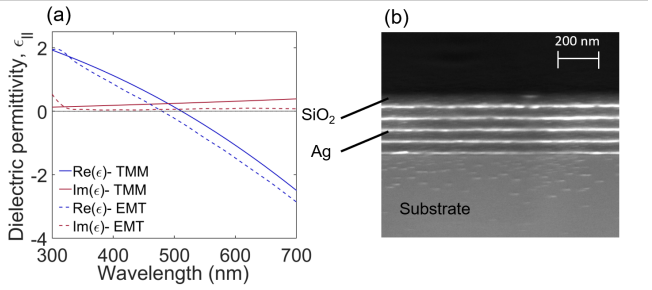

Figure 2: (a) Effective parallel permittivity, $\epsilon_{||}$, at normal incidence calculated using TMM and EMT for an Ag-SiO_2 multilayer stack with 5 bilayers of Ag (16 nm) and SiO_2 (65 nm). (b) Cross-sectional image of the fabricated Ag-SiO_2 multilayer stack taken with a scanning electron microscope.

substrate. The deposition rates of Ag and SiO_2 layers were kept at a low value of 0.1 nm/s in order to maintain film uniformity. To prevent oxidation, the top layer is the SiO_2 layer. A cross-section of the fabricated sample is shown in Fig. 2(b). Our fabricated sample agrees with our design within the usual fabrication tolerances.

The linear transmittance of the sample was probed using a collimated supercontinuum source covering the visible to NIR spectral range. We compared the measured transmission spectra to those predicted by TMM simulations for various metal and dielectric layer thicknesses. We found the best agreement with the experimental data for a metal-dielectric multilayer stack with thicknesses of 16 nm for Ag and 56 nm for SiO_2 (see supplemental materials for more details). The resulting zero-permittivity wavelength occurs at 470 nm, which is reasonably close to the predicted zero-permittivity wavelength of our device design (509 nm). The small discrepancy between the target zero-crossing wavelength and that determined from these linear characterization measurements is likely attributable to fabrication and measurement uncertainties.

We characterized the nonlinear optical properties of our sample using the Z-scan technique [2]. A schematic diagram of the experimental setup is shown in Fig. 3(a). We used pump pulses with a repetition rate of 50 Hz and a pulse duration of 28-ps from an optical parametric generator. Both closed- and open-aperture measurements were performed for wavelengths ranging from 410 nm to 560 nm. Note that the entire spectral range is in the ENZ region. All the measurements were conducted at normal incidence. Figures 3(b) and (c) show, respectively, representative closed-aperture and open-aperture signals from the Ag-SiO_2 multilayer stack at $\lambda = 500$ nm. The asymmetry in the closed-aperture signal with respect to the focus is due to the significant nonlinear absorption in the sample [33, 34]. We first extracted the imaginary part of the nonlinear phase shift from the open-aperture signal and used this value to calculate the real part of the phase shift from the closed-aperture signal. The extracted values of the real and imaginary nonlinear phase shifts were used in the standard expressions to calculate n_2 and β (see supplemental materials for details) [2]. For comparison, Figs. 3(b) and (c) also show similar measurements performed under the same conditions for a single 16-nm-thick Ag layer. Near the zero-permittivity wavelength, the accumulated nonlinear phase of the multilayer stack is 22 times larger than that of the 16-nm-thick silver layer, even though the multilayer stack contains only 5 times as much silver.

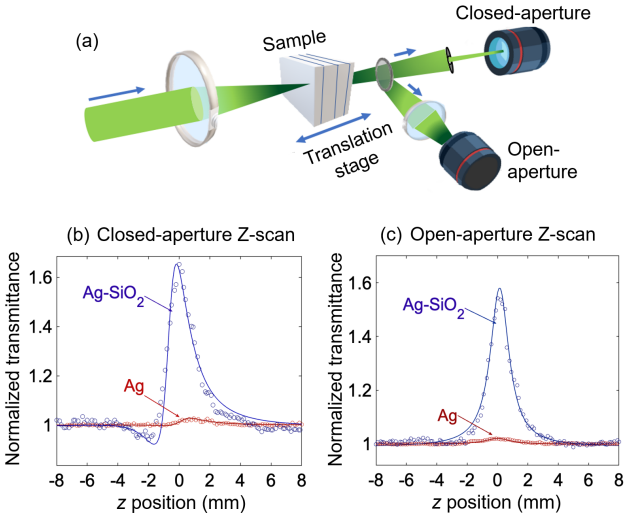

Figure 3: (a) Experimental setup. The Z-scan measurements were performed using 28-ps pulses with a repetition rate of 50 Hz from an optical parametric generator. A spatially filtered Gaussian beam is focused at normal incidence onto the sample by a lens. (b) The closed- and (c) open-aperture Z-scan signals at λ=500 nm for an Ag-SiO_2 multilayer stack (blue) and a thin film Ag layer (red) at normal incidence are shown. The solid lines represent theoretical fits to the experimental data.

The nonlinear refractive index n_2 and the nonlinear absorption coefficient β of the Ag-SiO_2 multilayer stack are shown as functions of wavelength in Figs. 4(a) and (b). It is clear that the nonlinear response is enhanced in the ENZ region of the spectrum, peaking at the zero-

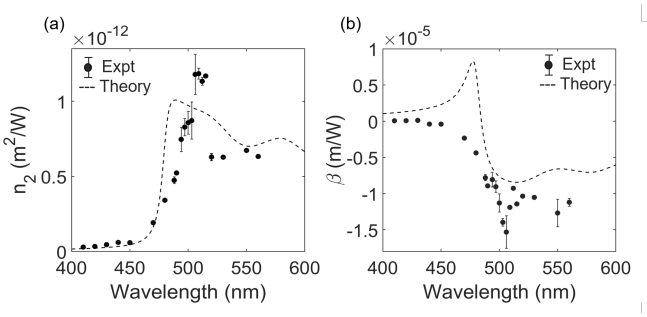

Figure 4: (a) The nonlinear refractive index n_2 and (b) the nonlinear absorption coefficient β of the Ag-SiO_2 multilayer stack as a function of wavelength. The dashed lines correspond to predictions from Eqs. (2) and (3) without any fit parameters.

permittivity wavelength targeted by this metamaterial design. The maximum measured phase shift at the zero-permittivity wavelength is $0.62\pi \pm 0.05$ rad. For the Ag-SiO_2 multilayer stack, the values of n_2 and β are $(1.2 \pm 0.1) \times 10^{-12}$ m^2/W and $(-1.5 \pm 0.2) \times 10^{-5}$ m/W, respectively. The peak value of the measured n_2 of the Ag-SiO_2 multilayer stack is 10^7 times larger than that of fused silica (3.2×10^{-20} m^2/W [35]), and is four times larger than that of an individual 16-nm-thick silver film (3×10^{-13} m^2/W).

We model the nonlinearity of the metamaterial stack using the nonlinear EMT [36]. Here, the effective nonlinear susceptibility of the metamaterial stack is the weighted average of the constituent materials. Since $\chi^{(3)}_{SiO_2}$ is much smaller than $\chi^{(3)}_{Ag}$, according to EMT, the dominant contribution to $\chi^{(3)}_{eff}$ of the metamaterial is from the Ag layers only (*e.g.*, $\chi^{(3)}_{eff} \approx \chi^{(3)}_{Ag} \times \rho$). We assume that $\chi^{(3)}_{Ag}$ is dispersionless over this spectral range. We measured our single silver layer sample at $\lambda = 500$ nm and obtained $\chi^{(3)} = (2.42 + 5.15i) \times 10^{-16}$ m^2/V^2, in good agreement with previously measured values [37,38]. The complex nonlinear response $\tilde{n}_2$ of the composite material is given by [35,39]

$$\tilde{n}_2 = \frac{3}{4\epsilon_0 c n_0 \mathrm{Re}[n_0]} \chi^{(3)}_{eff}, \quad (1)$$

where ϵ_0 is the vacuum permittivity and c is the speed of light in vacuum. Eq. (1) is related to the nonlinear refraction n_2 and the absorption coefficient β by the relations

$$n_2 = \mathrm{Re}[\tilde{n}_2] \quad (2)$$

$$\beta = \frac{4\pi}{\lambda} \mathrm{Im}[\tilde{n}_2]. \quad (3)$$

We plot these equations in Fig. 4 using the refractive index of our design as calculated by the EMT.

The model shows a strong, wavelength-dependent enhancement at the zero-permittivity wavelength that qualitatively resembles the experimental results. It correctly predicts the location and the maximum nonlinear response to within a factor of two without the need for any fit parameters or additional factors (*e.g.,* the slow-light factor $S = n_g/n_0$, where n_g is the group index [40,41]). The discrepancies in the breadth and the magnitude of this enhancement at the peak could likely be attributed to dimension variations between the design and the fabricated device, surface effects, imperfections in the constituent layers introduced during deposition, or our assumption that $\chi^{(3)}_{Ag}$ is dispersionless in our theoretical model. We note that our model predicts an additional peak for β at $\lambda = 475$ nm that we do not reproduce in the measurement and currently cannot account for. The qualitative agreement between such a simple theory and the experimental results suggests that this model may be used to predict and design the nonlinear optical response of other ENZ metamaterials.

In order to study the nature of the enhancement of the n_2 nonlinear response, we compare the response of the Ag-SiO_2 multilayer stack directly with that of a single thin film of silver. Given that $\chi^{(3)}_{eff} \approx \rho \times \chi^{(3)}_{Ag}$, with $\rho < 1$, any metamaterial stack composed of SiO_2 and Ag layers will exhibit a smaller $\chi^{(3)}$ value than that of silver. However, we found that at its peak the magnitude of n_2 of the metamaterial is four times that of silver. This observation implies that the ENZ condition increases n_2 to exceed the value of silver, despite the silver being "diluted" by a material with a lower nonlinearity (*i.e.*, SiO_2). This observation is further validated when comparing n_2 and β of the ENZ metamaterial at its zero-permittivity wavelength ($\lambda = 506$ nm) to these same values when $\epsilon_{eff} \approx 1$ ($\lambda = 410$ nm; see Fig. 2(a)). Here, the magnitudes of n_2 and β are increased in the ENZ region by factors of 40 and 250, respectively. In addition to this ENZ enhancement, at the zero-permittivity wavelength, the metamaterial has a smaller linear loss than silver ($\mathrm{Im}[n_0] = 0.3$ vs 3.1, respectively). Consequently, its effective propagation length can be much longer than that of silver (60 nm vs 9 nm), allowing for a much larger accumulation of nonlinear phase [42,43]. As shown by the peak-to-valley differences see in Fig. 3(b), in propagating through a 5-bilayer Ag-SiO_2 multilayer stack, the beam acquires a nonlinear phase shift that is approximately

22 times larger than that of the individual silver layer (1.53 rad vs 0.068 rad). Therefore, the benefit of using an ENZ metamaterial over a bulk metallic thin film are twofold: due to ENZ enhancement, and due to lowered loss [20, 22, 42, 43].

In conclusion, we have examined the nonlinear optical properties of an ENZ metamaterial realized through use of a metal-dielectric multilayer stack. This work further confirms that the enhancement of the nonlinear optical response that had previously been observed in homogeneous materials at the zero-permittivity wavelength [12, 13] occurs also in metamaterials at the zero of the *effective* permittivity [20–22]. We have observed that these materials produce a large nonlinear optical response and that the dominant mechanism for enhancing this response is the factor $1/(n_0 \mathrm{Re}[n_0])$. The ability to obtain strong nonlinearities at designated optical frequencies makes these metamaterials a flexible platform for applications in nonlinear optics.

There exists a broad variety of nonlinear optical phenomena, of which only the Kerr effect and saturable absorption were directly examined in this work. The investigation of other such nonlinear responses [44, 45] and their potential enhancement in ENZ metamaterials certainly warrants further study.

Acknowledgements This work was supported in part by the Canada First Research Excellence Fund, the Canada Research Chairs Program, and the Natural Sciences and Engineering Research Council of Canada (NSERC [funding reference number RGPIN/2017-06880]). R.W.B. acknowledges support from DARPA (grant No. W911NF- 18-0369) and ARO (ARO Grant W911NF-18-1-0337). O.R. acknowledges the support of the Banting Postdoctoral Fellowship from NSERC. Fabrication in this work was performed at the Centre for Research in Photonics at the University of Ottawa (CRPuO).

Author Contribution R.W.B conceived the basic idea for this work. O.R. performed the TMM simulations. J.U. fabricated the devices. S.S. built the experimental setup and carried out the measurements. S.S and Z.A. analyzed the experimental results. M.K aided with measurements and simulations. R.W.B. and O.R supervised the research and the development of the manuscript. S.S. wrote the first draft of the manuscript, and all authors subsequently took part in the revision process and approved the final copy of the manuscript. Portions of this work were presented at the Conference on Photonics North, FIO and Photonics West.

*Corresponding author: boydrw@mac.com

References

[1] Silveirinha, M. & Engheta, N. Tunneling of electromagnetic energy through subwavelength channels and bends using ϵ-near-zero materials. *Physical Review Letters* **97**, 157403 (2006).

[2] Adams, D. C. *et al.* Funneling Light through a Subwavelength Aperture with Epsilon-Near-Zero Materials. *Physical Review Letters* **107**, 133901 (2011).

[3] Prain, A., Vezzoli, S., Westerberg, N., Roger, T. & Faccio, D. Spontaneous Photon Production in Time-Dependent Epsilon-Near-Zero Materials. *Physical Review Letters* **118**, 133904 (2017).

[4] Alù, A., Silveirinha, M., Salandrino, A. & Engheta, N. Epsilon-near-zero metamaterials and electromagnetic sources : Tailoring the radiation phase pattern. *Physical Review B* **75**, 155410 (2007).

[5] Ciattoni, A., Rizza, C. & Palange, E. Transmissivity directional hysteresis of a nonlinear metamaterial slab with very small linear permittivity. *Optics Letters* **35**, 2130 (2010).

[6] Argyropoulos, C., Chen, P., D'Aguanno, G., Engheta, N. & Alù, A. Boosting optical nonlinearities in epsilon-near-zero plasmonic channels. *Physical Review B* **85**, 045129 (2012).

[7] Capretti, A., Wang, Y., Engheta, N. & Dal Negro, L. Enhanced third-harmonic generation in Si-compatible epsilon-near-zero indium tin oxide nanolayers. *Optics Letters* **40**, 1500–1503 (2015).

[8] Reshef, O., De Leon, I., Alam, M. Z. & Boyd, R. W. Nonlinear optical effects in epsilon-near-zero media. *Nature Reviews Materials* **4**, 535–551 (2019).

[9] P. B. Johnson & R. W. Christy. Optical Constants of the Noble Metals. *Physical Review B* **6**, 4370–4379 (1972).

[10] Wen, X. *et al.* Doubly Enhanced Second Harmonic Generation through Structural and Epsilon-near-Zero Resonances in TiN Nanostructures. *ACS Photonics* **5**, 2087–2093 (2018).

[11] Naik, G. V., Kim, J. & Boltasseva, A. Oxides and nitrides as alternative plasmonic materials in the optical range. *Optical Materials Express* **1**, 1090–1099 (2011).

[12] Alam, M. Z., De Leon, I. & Boyd, R. W. Large optical nonlinearity of indium tin oxide in its epsilon-near-zero region. *Science* **352**, 795–797 (2016).

[13] Caspani, L. *et al.* Enhanced nonlinear refractive index in epsilon-near-zero materials. *Physical Review Letters* **116**, 233901 (2016).

[14] Spitzer, W. G., Kleinman, D. & Walsh, D. Infrared properties of hexagonal silicon carbide. *Physical Review* **113**, 127–132 (1959).

[15] Kischkat, J. *et al.* Mid-infrared optical properties of thin films of aluminum oxide, titanium dioxide, silicon dioxide, aluminum nitride, and silicon nitride. *Applied Optics* **51**, 6789–6798 (2012).

[16] Edwards, B., Alù, A., Young, M. E., Silveirinha, M. & Engheta, N. Experimental verification of epsilon-near-zero metamaterial coupling and energy squeezing using a microwave waveguide. *Physical Review Letters* **100**, 033903 (2008).

[17] Hu, C. *et al.* Experimental demonstration of near-infrared epsilon-near-zero multilayer metamaterial slabs. *Optics Express* **21**, 23631–23639 (2013).

[18] Subramania, G., Fischer, A. J. & Luk, T. S. Optical properties of metal-dielectric based epsilon near zero metamaterials. *Applied Physics Letters* **101**, 241107 (2012).

[19] Maas, R., Parsons, J., Engheta, N. & Polman, A. Experimental realization of an epsilon-near-zero metamaterial at visible wavelengths. *Nature Photonics* **7**, 907–912 (2013).

[20] Neira, A. D. *et al.* Eliminating material constraints for nonlinearity with plasmonic metamaterials. *Nature Communications* **6**, 7757 (2015).

[21] Kaipurath, R. M. *et al.* Optically induced metal-to-dielectric transition in Epsilon-Near-Zero metamaterials. *Scientific Reports* **6**, 27700 (2016).

[22] Rashed, A. R., Yildiz, B. C., Ayyagari, S. R. & Caglayan, H. Hot Electron Dynamics in Ultrafast Multilayer Epsilon-Near-Zero Metamaterial. *Physical Review B* **101**, 165301 (2020).

[23] Wenshan, C. & Shalaev, V. Optical Metamaterials. *New York: Springer* **10** (2010).

[24] Kidwai, O., Zhukovsky, S. V. & Sipe, J. E. Effective-medium approach to planar multilayer hyperbolic metamaterials : Strengths and limitations. *Physical Review A* **85**, 053842 (2012).

[25] Newman, W. D. *et al.* Ferrell-berreman modes in plasmonic epsilon-near-zero media. *ACS Photonics* **2**, 2–7 (2015).

[26] Sihvola, A. H. Electromagnetic Mixing Formulae and Applications. *IET* **47** (1999).

[27] S. M. Rytov. Electromagnetic Properties of a Finely Stratified Medium. *Soviet Physics Jept* **2**, 466–475 (1956).

[28] West, P. R. *et al.* Searching for better plasmonic materials. *Laser and Photonics Reviews* **4**, 795–808 (2010).

[29] Palik, E. D. Handbook of optical constants of solids. *Academic Press* **3** (1998).

[30] Papadakis, G. T., Yeh, P. & Atwater, H. A. Retrieval of material parameters for uniaxial metamaterials. *Physical Review B* **91**, 155406 (2015).

[31] Smith, D. R., Vier, D. C., Koschny, T. & Soukoulis, C. M. Electromagnetic parameter retrieval from inhomogeneous metamaterials. *Physical Review E* **71**, 036617 (2005).

[32] Sheik-Bahae, M., Said, A. A., Wei, T. H., Hagan, D. J. & Van Stryland, E. W. Sensitive measurement of optical nonlinearities using a single beam. *IEEE Journal of Quantum Electronics* **26**, 760–769 (1990).

[33] Liu, X., Guo, S., Wang, H. & Hou, L. Theoretical study on the closed-aperture Z -scan curves in the materials with nonlinear refraction and strong nonlinear absorption. *Optics Communications* **197**, 431–437 (2001).

[34] Tsigaridas, G., Persephonis, P. & Giannetas, V. Effects of nonlinear absorption on the Z-scan technique through beam dimension measurements. *Materials Science and Engineering B* **165**, 182–185 (2009).

[35] Boyd, R. W. Nonlinear Optics. *Academic Press* **4th edn.** (2020).

[36] Boyd, R. W. & Sipe, J. E. Nonlinear optical susceptibilities of layered composite materials. *Journal of the Optical Society of America B* **11**, 297–303 (1994).

[37] Ma, G. & Tang, S. H. Ultrafast optical nonlinearity enhancement in metallodielectric multilayer stacks. *Optics Letters* **32**, 3435–3437 (2007).

[38] Yang, G., Guan, D., Wang, W., Wu, W. & Chen, Z. The inherent optical nonlinearities of thin silver films. *Optical Materials* **25**, 439–443 (2004).

[39] Sutherland, R. L. Handbook of Nonlinear Optics. *CRC press* (2003).

[40] Monat, C., De Sterke, M. & Eggleton, B. J. Slow light enhanced nonlinear optics in periodic structures. *Journal of Optics* **12**, 104003. (2010).

[41] Boyd, R. W. Material slow light and structural slow light: similarities and differences for nonlinear optics. *Journal of the Optical Society of America B* **28** (2011).

[42] Bennink, R. S., Yoon, Y., Boyd, R. W. & Sipe, J. E. Accessing the optical nonlinearity of metals with metal- dielectric photonic bandgap structures. *Optics Letters* **24**, 1416–1418 (1999).

[43] Lepeshkin, N. N., Schweinsberg, A., Piredda, G., Bennink, R. S. & Boyd, R. W. Enhanced nonlinear optical response of one-dimensional metal-dielectric photonic crystals. *Physical Review Letters* **93**, 123902 (2004).

[44] Luk, T. S. *et al.* Enhanced third harmonic generation from the epsilon-near-zero modes of ultrathin films. *Applied Physics Letters* **106**, 151103 (2015).

[45] Yang, Y. *et al.* High-harmonic generation from an epsilon-near-zero material. *Nature Physics* **15**, 1022–1026 (2019).

Supplemental Materials

This document provides supplementary information to "Enhanced nonlinear optical responses of layered epsilon-near-zero metamaterials at visible frequencies". In Sec. S1, we show the linear characterization of the sample. In Sec. S2, we describe the experimental procedure to ensure that the intensity distribution of the beam is Gaussian for the Z-scan measurements. In Sec. S3, we show the equations used for the retrieval of nonlinear coefficients n_2 and β from Z-scan measurements. Section S4 illustrates a change in sign of the nonlinear absorption in the operational wavelength range in the open-aperture Z-scan signals and Sec. S5 demonstrates asymmetry in the closed-aperture Z-scan signals in the operating wavelength range. In Sec. S6, we present the nonlinear phase shift as a function of irradiance.

S1 Linear characterization of the sample

The linear response of the Ag-SiO_2 multilayer stack is characterized by a transmission measurement at varying degrees of incidence. We compared the measured transmission spectra to those expected from the TMM simulations for several thicknesses of metal and dielectric layers in the stack. We found that the TMM simulations are consistent with the experimental data for a metal-dielectric multilayer stack with thickness of 16 nm of silver and 56 nm of SiO_2, as shown in Fig. S1

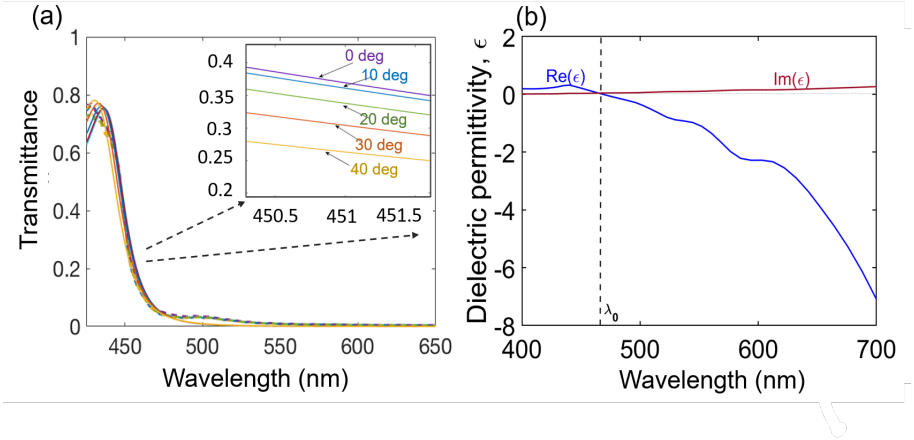

Figure S1: (a) Transmission spectra of the Ag-SiO_2 multilayer stack for p-polarization. The inset shows a zoomed-in view of the simulation spectra around 450 nm. The solid lines are the TMM simulation data and the dashed lines are the measurements. Colours represent different angles of incidence. (b) Dielectric permittivity of the Ag-SiO_2 multilayer stack calculated from transmission measurements.

S2 Beam cleaning

The Z-scan theory is based on the assumption that the incident beam is Gaussian (TEM00). Sometimes, the diffraction effects in the laser resonator cavity induces a change in the beam mode as it propagates outside the laser resulting in a non-Gaussian beam profile. The laser source used in our experiment produces a non-Gaussian beam. We adopted a spatial filtering technique to remove random fluctuations and higher order modes from the beam profile. The spatial filter set-up consists of a lens and a pinhole aperture attached to an $x-y-z$ positioning mechanism. By removing the higher order spatial modes inside the laser pulse, the spatial filter allows only Gaussian mode (TEM00) to pass through. Figure S1(a) and (b) shows the laser beam profile before and after the spatial filter, respectively.

Beam ellipticity e is another parameter which is of great importance in the Z-scan measurements. Large ellipticity values of the beam can badly affect the signal shape in Z-scan measurements. Wicksted *et al*. [1] studied the effects of beam ellipticity on Z-scan measurements and noticed that with an increase in ellipticity, both the peak and valley reduce from their symmetric maxima and minima that were attained in the circular limit ($e = 1$). We measure the beam ellipticity at different positions along the propagation length after spatial filtering the beam. Our filtered beam presents a good fit to a Gaussian as shown in Fig. S2(c) and (d) in x and y directions, respectively.

In the x-direction, the Gaussian fit to the experimental beam profile is 90.15% and in the y-direction it is 91.98%. The $1/e^2$ diameter of the input beam is 2959 μm in the x-direction and 2909 μm in the y-direction. From these values, we measure the ellipticity of the beam as 1.01.

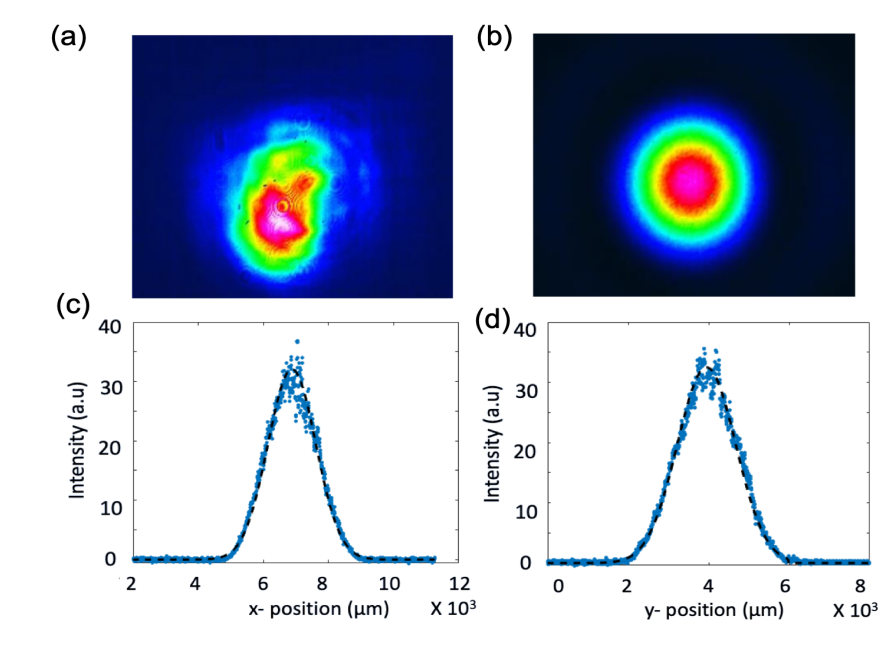

Figure S2: (a) Gaussian beam intensity profile (a) before and (b) after the spatial filter. Gaussian fit of the experimental beam profile in the (c) x- and (d) y- directions.

S3 Retrieval of nonlinear coefficients n_2 and β from Z-scan measurements

The nonlinear absorption coefficient β can be determined directly from the open-aperture measurements. In the open-aperture measurements, the aperture is removed and the total transmittance is collected using a lens. The variations in the transmission are largest at the focus and smallest away from it. For a beam with a Gaussian spatial profile, the transmission in the case of open-aperture is given by

$$T_{\mathrm{OA}} = 1 - \frac{\Delta\Psi}{1 + (z/z_0)^2}, \tag{S1}$$

where z_0 is the Rayleigh range and $\Delta\Psi$ is the imaginary part of nonlinear phase shift given by [2]

$$\Delta\Psi = \frac{\beta I_0 L_{\mathrm{eff}}}{2\sqrt{2}}, \tag{S2}$$

where β is the nonlinear absorption coefficient, I_0 is the peak intensity and L_{eff} is the effective sample thickness.

In the closed-aperture measurement, only a part of the intensity transmitted through the sample is collected. Thus, variations in the transmission correspond to both nonlinear absorption and nonlinear refraction. In the case of closed-

aperture, the transmission after the aperture is given by [2]

$$T_{\mathrm{CA}} = 1 + \frac{4(z/z_0)\Delta\Phi}{(1+(z/z_0)^2)(9+(z/z_0)^2)} - \frac{2((z/z_0)^2+3)\Delta\Psi}{(1+(z/z_0)^2)(9+(z/z_0)^2)} \tag{S3}$$

where $\Delta\Phi$ is the real part of nonlinear phase shift. $\Delta\Phi$ is related to the nonlinear refractive index n_2 by

$$\Delta\Phi = (1-S)^{0.25} k n_2 I_0 L_{\mathrm{eff}}, \tag{S4}$$

where $k = 2\pi/\lambda$ and S is the transmission through the aperture.
Therefore, by fitting the experimentally obtained open-and closed-aperture Z-scan transmission profiles with Eqs. (S1) and (S3), the nonlinear parameters n_2 and β can be found.

S4 Change in sign of the nonlinear absorption

Another interesting result is the change in sign of the nonlinear absorption coefficient as a function of wavelength. The change from reverse saturable absorption (RSA) to saturable absorption (SA) is observed at 440 nm. This is shown in Fig. S3. Below 450 nm RSA is observed and above 450 nm SA is observed. The physical mechanism behind this sign change is of interest for future research.

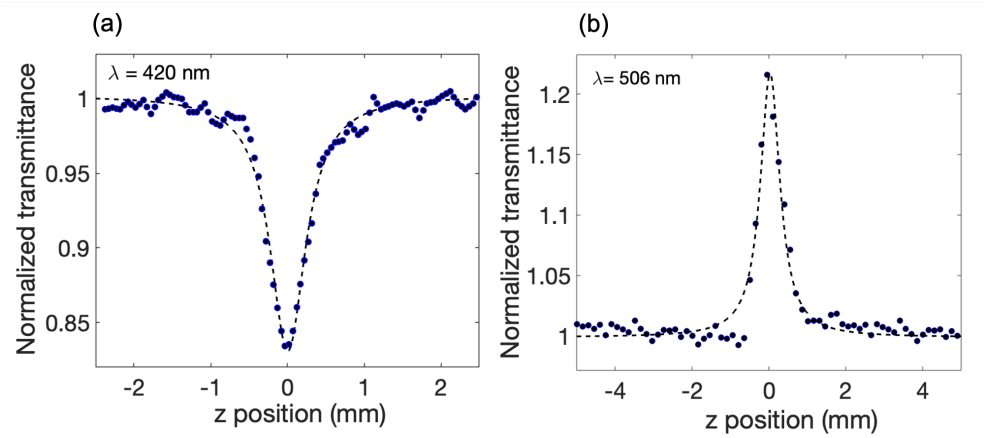

Figure S3: Open-aperture Z-scan signal showing a transition from reverse saturable to saturable absorption. (a) Reverse saturable absorption at 420 nm corresponding to a $\beta = 7.4 \times 10^{-8}$ m/W (b) Saturable absorption at 506 nm corresponding to a $\beta = -1.5 \times 10^{-5}$ m/W. We observed reverse saturable absorption for all operating wavelengths below 440 nm and saturable absorption for all wavelengths above 440 nm. The intensity at the focus was 300 MW/cm^2.

S5 Asymmetry in the closed-aperture Z-scan signal

Figure S4 shows the closed-aperture Z-scan signal measured at different wavelengths at and away from the zero-permittivity wavelength. As we can see from Fig. S4(a), at a shorter wavelength the closed-aperture Z-scan signal is symmetric with respect to the focus (*i.e*, at z=0). As we move towards the longer wavelength region, the closed-aperture signal loses its symmetry and becomes more asymmetric. This happens as a result of the large change in absorption at higher wavelengths. With an increase in the nonlinear absorption, the valley of the transmittance is severely suppressed and the peak is greatly enhanced, as shown in Figs. S4(b) and (c). The larger distortions in the Z-scan signal in the shorter wavelength region is due to the fluctuations in the OPG output in the lower wavelength limit.

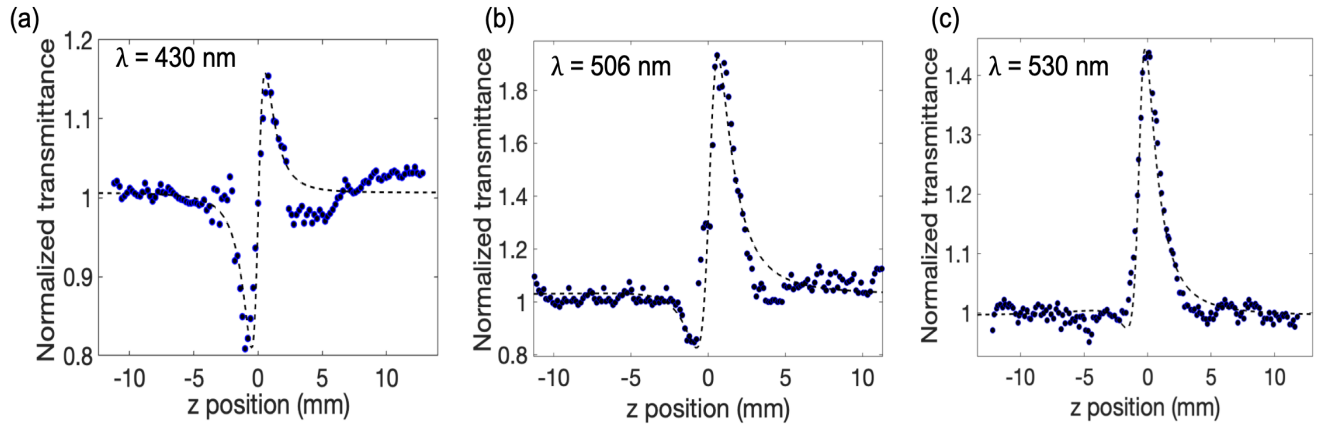

Figure S4: Closed-aperture Z-scan signal (a) at 430 nm (away from zero-permittivity wavelength, towards the blue side of spectrum) (b) at 506 nm (at the zero-permittivity wavelength) (c) at 530 nm (away from zero-permittivity wavelength, towards the red side of the spectrum).

S6 Nonlinear phase-shift

The main source of uncertainty in the value of n_2 is the absolute measurement of the irradiance. A plot of nonlinear phase shift $\Delta\Phi$ versus peak laser irradiance I_0 as measured from various Z-scan measurements at the same wavelength is shown in Fig. S5. The nonlinear phase-shift increases linearly with the irradiance on the sample. This in turn can also be used to find the damage threshold of the sample, which is at about 300 MW/cm^2.

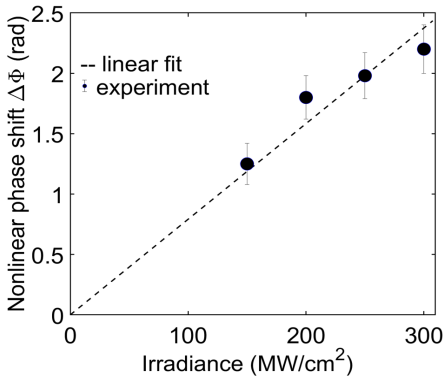

Figure S5: (a) Nonlinear phase shift as a function of the peak irradiance from the Z-scan data at λ=500 nm. The dashed line is a linear fit to the experimental data.

From Fig. S5, we calculated the slope of the linear fit. The nonlinear refractive index n_2 is determined using the equation slope= kn_2L_{eff}. The value of n_2 is therefore found to be 7.07×10^{-13} m^2/W at λ=500 nm, is very close to the value obtained by fits to individual Z-scan measurement traces (n2= $(8.5 \pm 0.7) \times 10^{-13}$ m^2/W). The experimental data is represented by the circles with each point has an error bar. The error bars were evaluated by calculating the standard error over 3 measurements.

A deviation from the linear behaviour could be the result of either higher-order nonlinearities or laser damage to the sample. In this experiment, we determined that the sample undergoes laser damage if the intensity goes above 300 MW/cm^2. So for all the experimental measurements, we set the intensity of the laser beam below 300 MW/cm^2 to avoid laser-induced damage.

References

[1] Mian, S. M., Taheri, B. & Wicksted, J. P. Effects of beam ellipticity on Z-scan measurements. *Josa B* **13**, 856–863 (1996).

[2] Sheik-Bahae, M., Said, A. A., Wei, T. H., Hagan, D. J. & Van Stryland, E. W. Sensitive measurement of optical nonlinearities using a single beam. *IEEE Journal of Quantum Electronics* **26**, 760–769 (1990).